Applied Surface Science 427 (2018) 649–655

Contents lists available at ScienceDirect

Applied Surface Science

journal homepage: www.elsevier.com/locate/apsusc

Full Length Article

Effect of flattened surface morphology of anodized aluminum oxide templates on the magnetic properties of nanoporous Co/Pt and Co/Pd thin multilayered films

T.N. Anh Nguyen[a,b,c,*], J. Fedotova[d], J. Kasiuk[d], V. Bayev[d], O. Kupreeva[e], S. Lazarouk[e], D.H. Manh[a], D.L. Vu[a], S. Chung[b,c], J. Åkerman[b,c], V. Altynov[f], A. Maximenko[d]

[a] Institute of Materials Science, Vietnam Academy of Science and Technology, 18 Hoang Quoc Viet, Hanoi, Viet Nam
[b] Material Physics Department, Royal Institute of Technology, 164 40 Kista, Sweden
[c] Department of Physics, University of Gothenburg, Gothenburg, 41296, Sweden
[d] Institute for Nuclear Problems, Belarusian State University, Minsk, Belarus
[e] Belarusian State University of Informatics and Radioelectronics, Minsk, Belarus
[f] Joint Institute for Nuclear Research, 141980 Dubna, Moscow region, Russia

ARTICLE INFO

Article history:
Received 27 March 2017
Received in revised form 19 August 2017
Accepted 31 August 2017

Keywords:
Antidots
Perpendicular magnetic anisotropy
Percolated perpendicular media
Co/Pd multilayers
Co/Pt multilayers
Porous anodic aluminum oxide templates

ABSTRACT

For the first time, nanoporous Al_2O_3 templates with smoothed surface relief characterized by flattened interpore areas were used in the fabrication of Co/Pd and Co/Pt multilayers (MLs) with strong perpendicular magnetic anisotropy (PMA). Alternating gradient magnetometry (AGM) revealed perfectly conserved PMA in the Co/Pd and Co/Pt porous MLs (antidot arrays) with a ratio of remanent magnetization (M_r) to saturation magnetization (M_S) of about 0.99, anisotropy fields (H_a) of up to 2.6 kOe, and a small deviation angle of 8° between the easy magnetization axis and the normal to the film surface. The sufficient magnetic hardening of the porous MLs with enhanced coercive field H_C of up to ~1.9 kOe for Co/Pd and ~1.5 kOe for Co/Pt MLs, as compared to the continuous reference samples (~1.5–2 times), is associated with the pinning of the magnetic moments on the nanopore edges. Application of the Stoner–Wohlfarth model for fitting the experimental $M/M_S(H)$ curves yielded clear evidence of the predominantly coherent rotation mechanism of magnetization reversal in the porous films.

1. Introduction

Nanopatterned Co/Pd and Co/Pt multilayers (MLs) possessing perpendicular magnetic anisotropy offer great opportunities for basic studies of nanomagnetism [1–5], as well as for various applications, such as magnetic sensors, magnetic random access memory, magnetic logic devices, and media for high-density recording [6–11]. However, attempts to fabricate high-density perpendicular recording media face serious limitations because of the superparamagnetic effect — that is, the undesirable thermal fluctuations of magnetic moments when the grain size falls to a few nanometers [12]. The formation of percolated perpendicular media containing exchange-coupled MLs with densely distributed pinning centers (nanopores) allows this restriction to be overcome [13,14].

The fabrication of nanopatterned thin films by means of lithographic techniques requires expensive equipment and multiple processing steps [9,15–18], which may not be suitable for large-scale device fabrication. Another approach to nanopatterning that utilizes anodized porous templates (Al_2O_3, ZrO_2, and TiO_2) appears to be particularly encouraging for the fabrication of porous exchange-coupled MLs [19,20]. It has been well established that Co/Pd and Co/Pt MLs fabricated on porous templates with a developed U-shape morphology (Al_2O_3, nanospheres) typically have disturbed magnetic anisotropy and a poor ratio between remanent M_r and saturation M_S magnetizations, originating from local misalignment of perpendicularly oriented magnetic moments on curved surfaces [21,22]. With respect to this, the deposition of MLs on smoothed-relief porous templates results in better conservation and adjustment of PMA in nanoporous MLs. To that end, we deposited Co/Pt and Co/Pd MLs on the templates of Al_2O_3, where specifically selected anodization regimes and subsequent surface

* Corresponding author at: Institute of Materials Science, Vietnam Academy of Science and Technology, 18 Hoang Quoc Viet, Hanoi, Viet Nam.
E-mail address: ngocanhnt.vn@gmail.com (T.N.A. Nguyen).

http://dx.doi.org/10.1016/j.apsusc.2017.08.238
0169-4332/

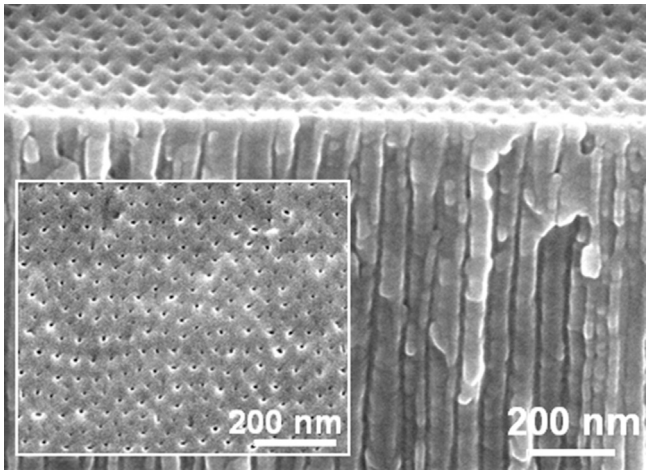

Fig. 1. SEM image of the initial template of anodized Al_2O_3 taken at an angle of 45° with respect to the sample surface; the inset shows a top-view image of the template surface.

Ar ion etching allow the interpore areas to be flattened and the relief gradient to be reduced.

The aim of this work is to investigate the effect of the flat-surface morphology of Al_2O_3 templates on the magnetic characteristics of Co/Pd and Co/Pt MLs fabricated over such matrices.

2. Experimental

Templates of nanoporous Al_2O_3 were fabricated by two-stage anodization of Al film (0.4 μm) in 2% sulfuric acid aqueous solution at room temperature. Al foil was deposited over Si wafer by magnetron sputtering. The anodization voltage was linearly increased from zero to 25 V at 1 V/s and then held constant for the total anodization time, which was no longer than 35 min. The end of the anodization process was monitored by the drop of the anodic current below 30% of its maximum value. Subsequent Ar ion-plasma etching for 60 min was used to additionally flatten the surface relief.

Co/Pd and Co/Pt MLs with nominal composition $Pd_{15nm}/[Co_{0.5nm}/Pd_{1nm}]_{x5}/Pd_{3nm}$ and $Pt_{15nm}/[Co_{0.4nm}/Pt_{0.8nm}]_{x5}/Pt_{3nm}$, and with 5 nm Ta buffer and capping layers, were deposited over anodized Al_2O_3 templates. In addition to the nanopatterned samples, the same MLs were also deposited on Si/SiO_2 substrates in order to obtain continuous films as references. These MLs were fabricated using an ultra-high vacuum magnetron sputtering system (AJA International, Inc., USA) with a base pressure below 3×10^{-8} Torr. The Ar gas pressure was kept at 5 mTorr during sputtering for the Co, Pt, and Pd layers and at 2 mT for the Ta layers. All layers were deposited at room temperature, with deposition rates of 0.2, 0.35, 0.3, and 0.7 Å/s for Co, Pt, Pd, and Ta, respectively. The Pd/Ta and Pt/Ta bilayers were used as capping layers for preventing oxidation of the MLs, while the Ta/Pd and Ta/Pt bilayers were applied to promote the (111) texture of the MLs [23,24]. The layer thicknesses were determined from the deposition time and calibrated deposition rates.

The surface morphology and cross-sectional microstructure of the templates and films were examined using a Hitachi S-4800 scanning electron microscope (SEM) at a voltage of 15 kV and an NT-MDT Solver-Pro 47 atomic force microscope (AFM) using an NSG01 DLC supersharp diamondlike carbon tip with a curvature radius below 3 nm. The chemical composition of the films was examined using X-ray photoelectron spectroscopy (XPS) with a K Alpha spectrometer (Thermo Fisher Scientific) with a base pressure in the chamber of 7×10^{-7} Pa. Photoelectrons were excited by Al-K_α (1486 eV) with a beam diameter of 400 μm. All samples were etched using an Ar^+ ion beam with an energy of 200 eV to remove carbon and oxygen contamination from the surface. The spectra were analyzed using Avantage software (Thermo Fisher Scientific). The films structure was examined by X-ray powder diffraction (XRD) using an X'pert Pro X-ray diffractometer at a voltage of 45 kV and a current of 40 mA with Cu-K_α X-ray radiation ($\lambda = 0.15418$ nm). The magnetic properties of the patterned and unpatterned PMA films were characterized using an alternating gradient magnetometer (AGM) up to 1.4 T at room temperature.

3. Results and discussion

The surface morphology of the nanoporous Al_2O_3 templates was examined by SEM. Fig. 1 shows an SEM image of the initial template of anodized Al_2O_3 taken at an angle of 45° with respect to the sample surface; the inset is a top-view SEM image. These images clearly illustrate that nanopores with an average diameter *D* of about 20 nm are homogeneously distributed over the perfectly smoothed surface of anodized Al_2O_3. It is worth noticing that the surface morphology obtained, with its flattened interpore areas, is very different from the pronounced U-shaped relief (with surface roughness of up to 20 nm) of the Al_2O_3 templates that are typically used in the preparation of arrays of magnetic antidots [25].

SEM images of the Co/Pd and Co/Pt fabricated over the Al_2O_3 templates are presented in Fig. 2 (a) and (b), respectively; they show the porous structure of the magnetic MLs with average estimated *D* values of about 20 nm. Generally, the morphology of Co/Pd

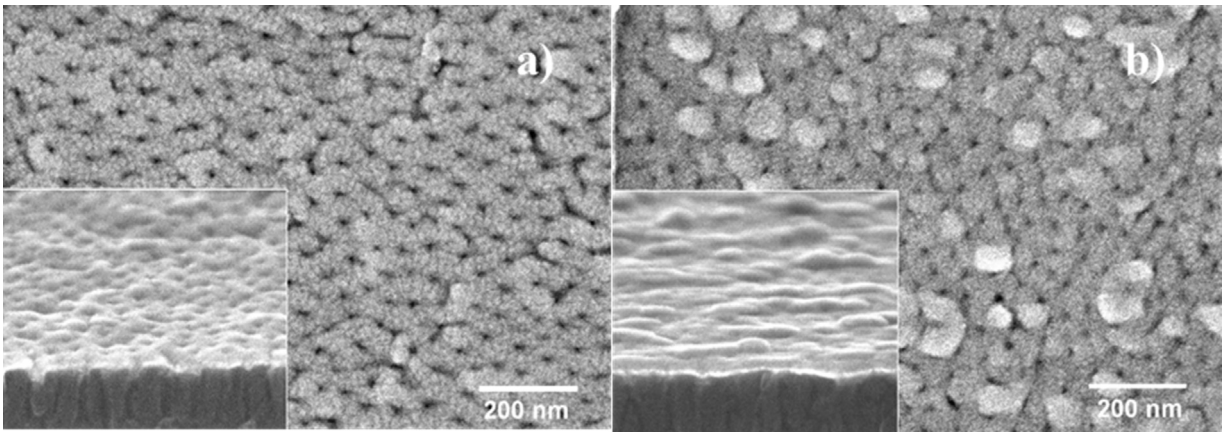

Fig. 2. Top-view SEM images of Co/Pd (a) and Co/Pt (b) porous MLs deposited over Al_2O_3 templates; the insets show surface images taken at an angle of 45° to the sample surface.

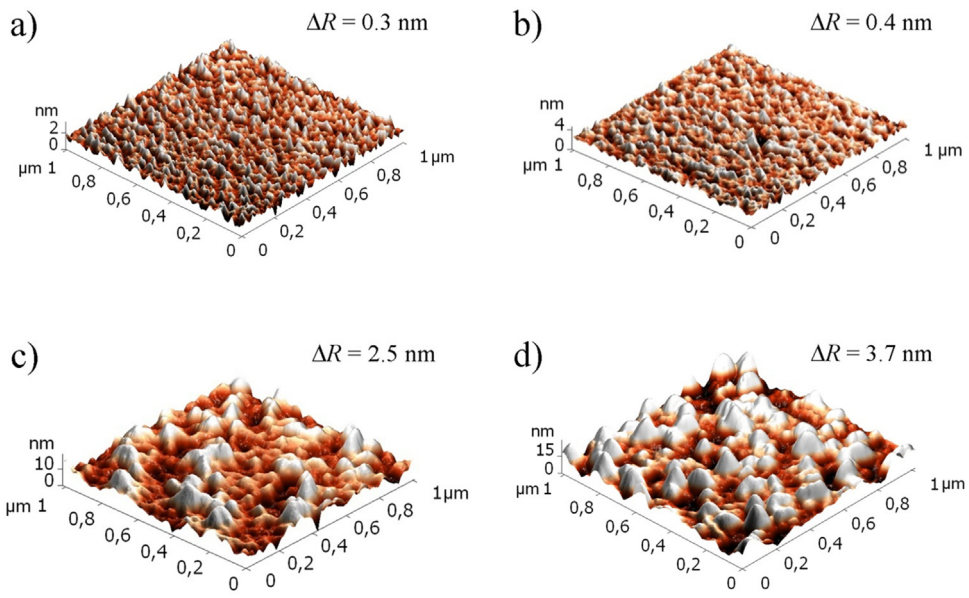

Fig. 3. 3D AFM images of Co/Pd (a, c) and Co/Pt (b, d) MLs deposited over flat Si/SiO_2 wafers (a, b) and porous Al_2O_3 templates (c, d); the ΔR parameter indicates the average surface roughness of the films.

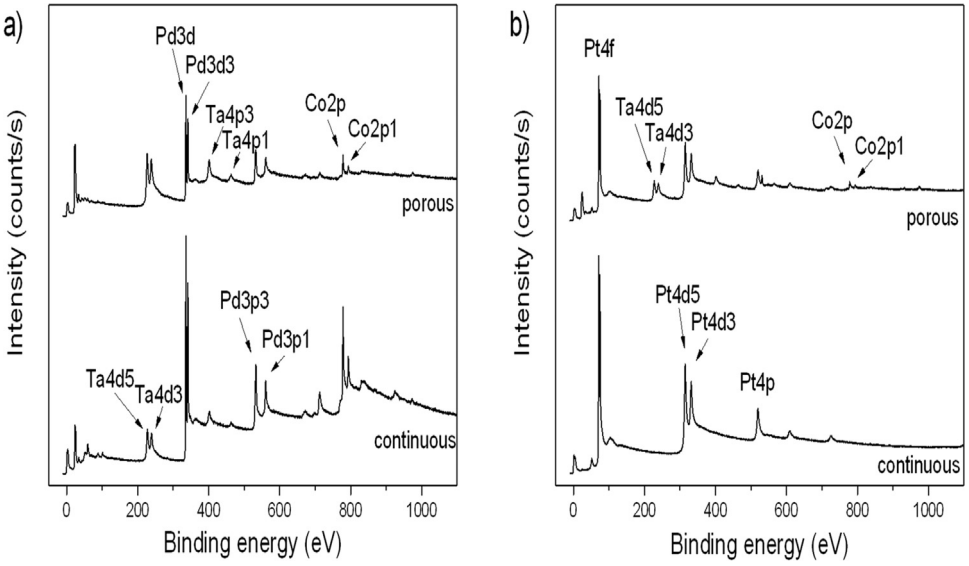

Fig. 4. Survey XPS spectra of Co/Pd (a) and Co/Pt (b) MLs deposited over flat Si/SiO_2 wafers and porous Al_2O_3 templates.

porous films is quite smooth due to the lower relief of the initial template. However, the surface of the Co/Pt MLs is characterized by irregularly distributed flattened grains with spatial sizes of about 50–100 nm in the film plane.

The relief of Co/Pd and Co/Pt MLs fabricated over flat Si/SiO_2 wafers and porous anodized Al_2O_3 templates was analyzed using AFM (Fig. 3). As shown in Fig. 3(a) and (b), the surface of multilayered films on Si/SiO_2 wafers is characterized by smoothed relief and low average roughness ΔR of 0.3 nm for Co/Pd and 0.4 nm for Co/Pt systems. The AFM images of the corresponding porous systems presented in Fig. 3(c) and (d) reveal more complicated film morphology, including detectable pores and surface inhomogeneities, in agreement with SEM data. Nevertheless, the average surface roughness of the porous systems is rather low (ΔR = 2.5 nm and 3.7 nm for Co/Pd and Co/Pt porous films) indicating that a reasonably flat surface could be obtained by deposition on porous Al_2O_3 templates.

The chemical composition of the multilayered Co/Pd and Co/Pt films fabricated over flat Si/SiO_2 wafers and porous anodized Al_2O_3 templates was analyzed layer by layer by XPS. The corresponding spectra were detected after etching approximately every 0.3 nm of the films. Typical survey spectra obtained after etching Ta and Pd (or Pt) capping layers — that is, "inside" the Co/Pd and Co/Pt MLs — are presented in Fig. 4. As can be seen, Pd (or Pt) and Co are the dominating elements in both the Co/Pd and Co/Pt MLs. Their estimated atomic ratio equals n(Co):n(Pd) = 52:48 at.% and n(Co):n(Pt) = 24:76 at.%. Following etching, the Co concentration decreases and is gradually eliminated when the Pd (or Pt) buffer layer is reached.

High resolution XPS spectra in the region of the Co2p line are shown in Fig. 5 for Co/Pd and Co/Pt MLs. The positions of $Co2p_{3/2}$ and $Co2p_{3/2}$ lines at 778.2 eV and 793.3 eV, respectively, indicate that Co is in a metallic state in both the Co/Pd and Co/Pt system [26]. It should be emphasized that the positions of the Co2p lines coincide excellently for the continuous and porous films.

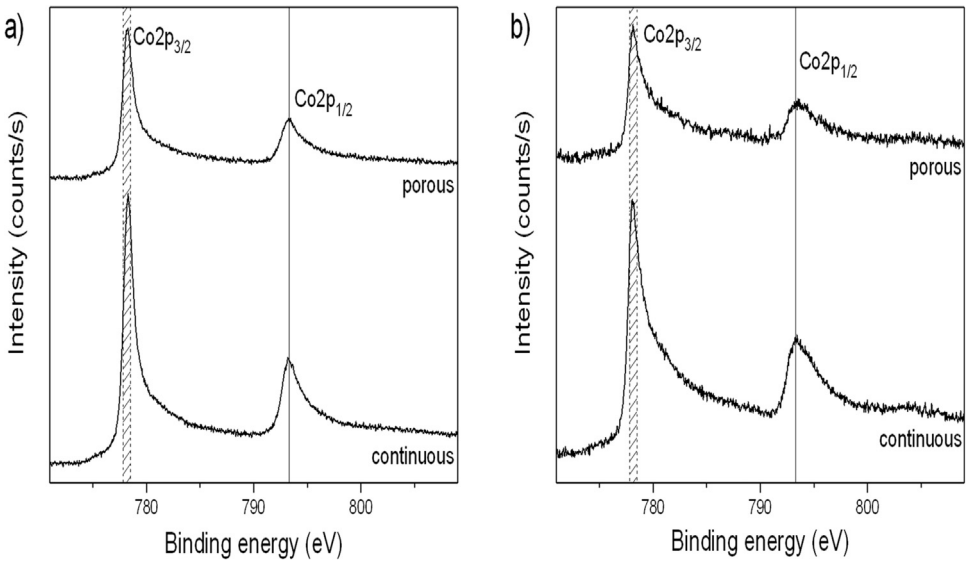

Fig. 5. High-resolution XPS spectra in the region of the Co2p line for Co/Pd (a) and Co/Pt (b) MLs deposited over flat Si/SiO_2 wafers and porous Al_2O_3 templates; the shaded regions correspond to literature data on Co2p line positions of bulk Co [26].

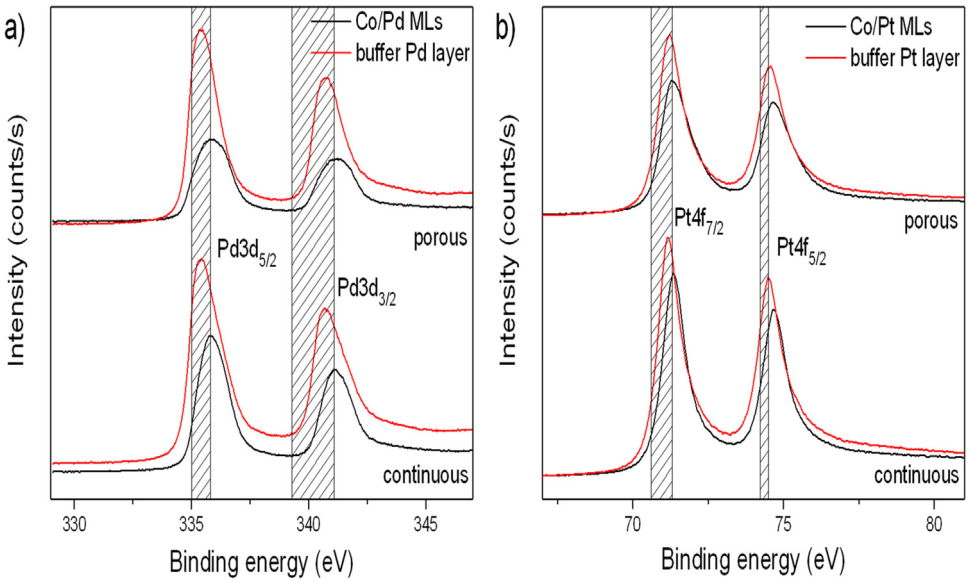

Fig. 6. High-resolution XPS spectra in the region of Pd3d and Pt4f lines for Co/Pd (a) and Co/Pt (b) MLs deposited over flat Si/SiO_2 wafers and porous Al_2O_3 templates; the shaded regions correspond to literature data on Pd3d and Pt4f line positions of bulk Pd and Pt [26].

Fig. 6 shows the high resolution XPS spectra in the region of the Pd3d and Pt4f lines, obtained "inside" the Co/Pd and Co/Pt MLs as well as after Co/Pd and Co/Pt MLs etching — that is, in pure Pd and Pt buffer layers. Comparison of these spectra allows changes to be revealed in the local surrounding of Pd (or Pt) atoms inside the MLs system, as compared to the pure Pd (or Pt). As can be seen from Fig. 6, there is an evident shift of Pd (and Pt) lines towards higher energies with respect to pure Pd (or Pt), which occurs in the spectra obtained inside the MLs, both in continuous and porous films. This shift indicates CoPd (or CoPt) alloy formation [27,28]. The coincidence of the $Co2p_{3/2}$ line position with the bulk metallic Co [26], accompanied with the shift in the Pd3d and Pt4f lines, points to polarization of Pd and Pt by Co atoms in the CoPd (or CoPt) alloy.

The experimental XRD patterns of both antidots and continuous (reference sample) Co/Pd and Co/Pt MLs are presented in Fig. 7(a) and (b), respectively. As Fig. 7(a) shows, the continuous Co/Pd film demonstrates two clear intense diffraction lines at 39.9° and 41.1°, corresponding well to the position of the main (111) peaks of the *fcc* structure of Pd (2θ~40°) [25,29] and of the Co_xPd_{1-x} quasi-alloy (2θ~40.7–41.1°) [25,30–32]. The partial overlap of these diffraction lines, as well as some intermediate peaks at 2θ~40.3°, should be pointed out. The dominating Pd (111) line is mainly from the Pd buffer and capping layers, whereas the additional diffraction lines at higher 2θ values correspond to the phase that appears as the result of interface mixed layer among the Co and Pd layers, and the incorporation of Co into the Pd layers [25,33]. The presence of two additional reflections at $2\theta = 40.3°$ and 41.1° indicates the possible formation of Co_xPd_{1-x} quasi-alloy with variable composition and lattice parameter *a* [30]. Similar results were also observed in the nanoporous Co/Pd MLs. The diffraction peaks at 2θ~39.9–41.1° can reasonably be associated with the formation of a Co_xPd_{1-x} quasi-alloy [30]. The XRD patterns of the continuous and porous Co/Pt MLs (see Fig. 7(b)) have the most intense diffraction line at 39.8°; this corresponds to the bulk *fcc* Pt (111) (2θ~39.7°–40.0° [34,35])

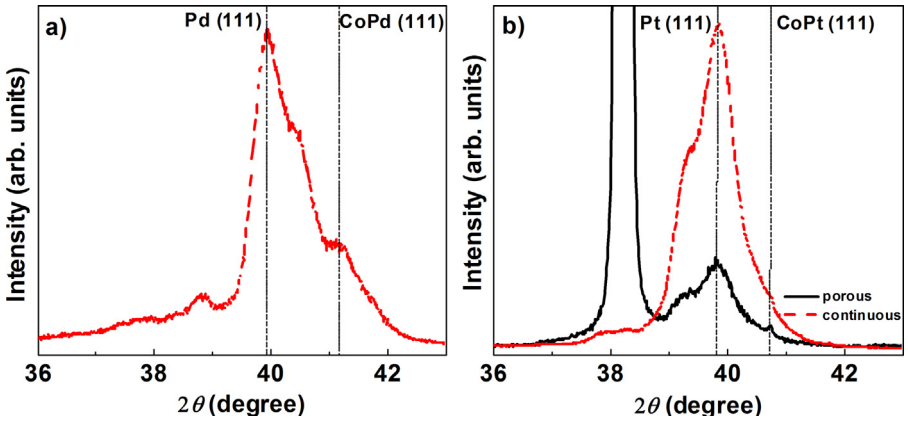

Fig. 7. XRD patterns of Co/Pd (a) and Co/Pt (b) multilayered films on porous anodized Al_2O_3 templates (solid lines) and flat Si/SiO_2 wafers (dashed lines).

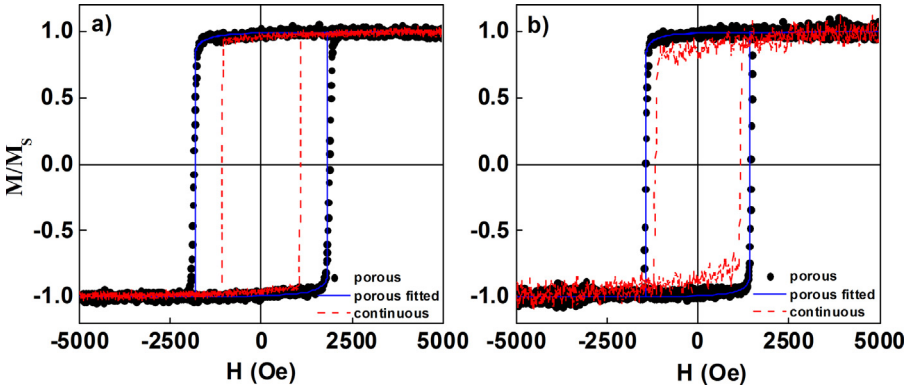

Fig. 8. Normalized magnetization curves of Co/Pd (a) and Co/Pt (b) MLs on nanoporous anodized Al_2O_3 templates (dots) and flat Si/SiO_2 wafers (dashed lines); the solid lines shows approximations of experimental M/MS(H) curves of the porous films in accordance with the Stoner–Wohlfarth model [38].

diffraction line. Another wide peak at 40.5° overlaps with the Pt (111) line and is associated with the (111) diffraction line of the *fcc* CoPt (111) alloy (2θ~40.5° [36]). The intense diffraction line at 2θ~39.4° indicates a disordered Pt phase [37].

Fig. 8(a) and (b) shows the experimental field dependencies of the normalized magnetization $M/M_S(H)$ for nanoporous (black dots) and continuous (red lines) Co/Pd and Co/Pt films, measured in an external magnetic field H applied along the normal to the film surface. The magnetization curves of the continuous films demonstrate high values for the magnetic squareness ratio M_r/M_S, equaling 0.96 for the Co/Pd system and 0.87 for the Co/Pt film. This observation, coupled with the sufficiently high coercive field H_C of the films in this direction of about 1.1 kOe, indicates that the films are characterized by pronounced PMA [25,33].

Remarkably, Fig. 8 reveals that both the Co/Pd and Co/Pt porous MLs also possess a perfect M_r/M_S value of 0.99, which provides evidence of conservation of PMA, despite the engraved nanoporous structure of their surfaces. Additionally, compared with the continuous films grown on silicon, the nanoporous films exhibit much larger values for the coercive force. H_C increases from 1.1 kOe (continuous film) to ~1.9 kOe (nanoporous film) for Co/Pd MLs, and from 1.2 kOe (continuous film) to 1.5 kOe (nanoporous film) for Co/Pt MLs, revealing significant magnetic hardening for the porous MLs. The increase by a factor of ~1.5–2 in the H_C of the porous films is governed by *i*) hindering of the propagation of the domain wall motion [39] and *ii*) change in the magnetization reversal process [33], both of which are induced by the films' porosity. It is generally accepted that the increase of H_C in nanoporous films is associated with the pinning of the magnetic moments at the nanopore edges during magnetization reversal [39]. The change in the magnetization reversal mechanism is often observed in various porous films characterized by nanosized pores with small distances between them [33,39]. It is well established that continuous multilayered films with PMA demonstrate domain wall motion as their dominant magnetization reversal mechanism. This is well described by the modified Kondorski model [40]. Nanostructured porous films formed as the result of sputtering on porous substrates are often characterized by rotational mechanisms of magnetization reversal (coherent or incoherent rotation of magnetic moments) [33,39] or a combination of rotational mechanisms with domain wall motion.

For a more thorough understanding of the underlying magnetization mechanism, a theoretical approach was taken. The Stoner–Wohlfarth (SW) model, or coherent rotation model, is the simplest model for describing magnetization reversal processes by the rotation of magnetic moments. It has been successfully used for numerous multilayered systems [41], including porous films [33,42,43] and was applied here to simulate the hysteresis loops [38]. The results of approximation of the experimental $M/M_S(H)$ dependencies of the Co/Pd and Co/Pt porous films, using this model, are presented in Fig. 8. Details of approximation are described in [33]. In accordance with the Stoner–Wohlfarth model, the $M/M_S(H)$ curve can be fitted with a theoretical dependence $\cos\theta(h)$, which is the solution of the equation [38]:

$$h \cdot sin\theta + \frac{1}{2}\sin\left(2\left(\theta - \alpha\right)\right) = 0,$$

where $h = H/H_a$ is the normalized magnetic field, H_a is the effective anisotropy field of the films, θ is the angle between the magnetic moment of the films and the external magnetic field H, and α is the angle between the films' easy magnetization axis and H (i.e. the

film's normal). Fig. 8 shows the perfect agreement of experimental and modeled curves for both Co/Pd and Co/Pt MLs. This indicates the applicability of this model to the porous MLs being examined and the presence of the rotational modes in their magnetization reversal process. Moreover, the approximation allows estimation of the value of the anisotropy field H_a characterizing the PMA of the porous films. Calculations show that H_a = 2.6 kOe for Co/Pd and 2.0 kOe for Co/Pt porous MLs. The average angle α of deviation of the easy magnetization axis of the porous films from their normals appears to be 8° for both systems, according to the approximation results. The origin of such deviations lies in the local morphology inhomogeneities of the porous films related to nanopore edges [33]. Thus, the rather low value of the α parameter extracted from the modeled curves confirms the perfect conservation of the high PMA effect in the porous MLs examined here.

4. Summary

For the first time, flat-surface porous templates of Al_2O_3 have been used in the fabrication of Co/Pd and Co/Pt MLs characterized by strong PMA. SEM characterization of porous Al_2O_3 templates anodized under specifically selected regimes with subsequent Ar ion etching confirms the flattening of interpore areas on the template surface, leading to smoothed morphology of Co/Pd and Co/Pt MLs. The phase composition of porous MLs studied by XRD and XPS shows the formation of CoPd and CoPt alloys.

The magnetization curves $M/M_S(H)$ recorded under an external perpendicular magnetic field reveal a perfectly conserved PMA in both porous MLs. That is shown by the high value of $M_r/M_S \approx 0.99$. An increase by a factor of about two in the coercive field H_C, up to the 1.9 kOe observed in porous Co/Pd and Co/Pt MLs with respect to their continuous counterparts is related to the pinning of the magnetic moments at the nanopore edges.

The experimental $M/M_S(H)$ dependencies recorded for porous MLs were successfully approximated with theoretical curves within the frame of the Stoner–Wohlfarth model, which indicates a predominantly coherent rotation mechanism of magnetization reversal. In addition, the high anisotropy fields H_a (of up to 2.6 kOe) and small deviation angle α (up to 8°) of the easy magnetization axis from normal to the film surface extracted from the fitted curves confirm that deposition of MLs over flat-surface porous Al_2O_3 templates promotes the conservation of PMA in porous MLs.

Acknowledgments

We acknowledge financial support from the Vietnam Academy of Science and Technology under project VAST.HTQT.BELARUS.03/16-17 and from the National Foundation for Science and Technology Development of Vietnam under Project 103.99-2015.83. J. Fedotova acknowledges support from the grant of the President of the Republic of Belarus State and the Research Program entitled "Physical materials science, new materials and technologies" (task 2.44) and the Belarusian Republic Foundation for Basic Research (project no. F16V2-004). J. Kasiuk acknowledges support from the World Federation of Scientists. J. Åkerman acknowledges support from the Swedish Foundation for Strategic Research (SSF), the Swedish Research Council (VR), the Göran Gustafsson Foundation, and the Knut and Alice Wallenberg Foundation (KAW).

References

[1] G. Hu, T. Thomson, C.T. Retter, S. Raoux, B.D. Terris, Magnetization reversal in Co/Pd nanostructures and films, J. Appl. Phys. 97 (2005) 10J702.
[2] S. Okamoto, T. Kato, N. Kikuchi, O. Kitakami, N. Tezuka, S. Sugimoto, Energy barrier and reversal mechanism in Co/Pt multilayer nanodot, J. Appl. Phys. 103 (2008) 07C501.
[3] M. Delalande, J. de Vries, L. Abelmann, J.C. Lodder, Measurement of the nucleation and domain depinning field in a single Co/Pt multilayer dot by anomalous Hall effect, J. Magn. Magn. Mater. 324 (7) (2012) 1277–1280.
[4] K.F. Huang, J.W. Liao, C.Y. Hsieh, L.W. Wang, Y.C. Huang, W.C. Wen, M.T. Chang, S.C. Lo, J. Yuan, H.H. Lin, C.H. Lai, Magnetic patterning: local manipulation of the intergranular exchange coupling via grain boundary engineering, Sci. Rep. 5 (2015) 11904.
[5] E. Chunsheng, V. Parekh, P. Ruchhoeft, S. Khizroev, D. Litvinov, Magnetization reversal in patterned $(Co/Pd)_n$ multilayers, J. Appl. Phys. 103 (2008) 063904.
[6] Judith Kimling née Moser, Vojko Kunej, Hans-Fridtjof Pernau, Elke Scheer, Manfred Albrecht, Magnetoresistive effects in Co/Pd multilayers on self-assembled nanoparticles, J. Appl. Phys. 107 (9) (2010) 09C06.
[7] A. Moser, K. Takano, D.T. Margulies, M. Albrecht, Y. Sonobe, Y. Ikeda, S. Sun, E.E. Fullerton, Topical review: magnetic recording: advancing into the future, J. Phys. D: Appl. Phys. 35 (19) (2002) R157–R167.
[8] M. Abes, M.V. Rastei, J. Venuat, A. Carvalho, S. Boukari, E. Beaurepaire, P. Panissod, A. Dinia, J.P. Bucher, V. Pierron-Bohnes, Magnetic switching field distribution of patterned CoPt dots, J. Appl. Phys. 105 (2009) 113916.
[9] J.S. Sohn, D. Lee, E.H. Cho, H.S. Kim, B.K. Lee, M.B. Lee, S.J. Suh, The fabrication of Co–Pt electro-deposited bit-patterned media with nanoimprint lithography, Nanotechnology 20 (2) (2008) 025302.
[10] M. Huda, Z.B. Mohamad, T. Momori, Y. Yin, S. Hosaka, Fabrication of CoPt nanodot array with a pitch of 33 nm using pattern-transfer technique of PS-PDMS self-assembly, Key. Eng. Mater. 596 (2013) 83–87.
[11] O. Hellwig, T. Hauet, T. Thomson, E. Dobisz, J.D. Risner-Jamtgaard, D. Yaney, B.D. Terris, E.E. Fullerton, Coercivity tuning in Co/Pd multilayer-based bit-patterned media, Appl. Phys. Lett. 95 (2009) 232505.
[12] C.P. Bean, J.D. Livingstone, Superparamagnetism, J. Appl. Phys. 30 (1959) 120S.
[13] Jian-Gag Zhu and Yuhiu Tang, A medium microstructure for high area density perpendicular recording, J. Appl. Phys. 99 (2006) 08Q903.
[14] D. Suess, J. Fidler, K. Porath, T. Schrefl, D. Weller, Micromagnetic study of pinning behavior in percolated media, J. Appl. Phys. 99 (2006) 08G905.
[15] C.A. Ross, Patterned magnetic recording media, Annu. Rev. Mater. Res. 31 (2001) 203.
[16] C.T. Rettner, S. Anders, J.E.E. Baglin, T. Thomson, B.D. Terris, Characterization of the magnetic modification of Co/Pt multilayer films by He^+ Ar^+, and Ga^+ ion irradiation, Appl. Phys. Lett. 80 (2002) 279.
[17] Y. Hao, F.J. Castano, C.A. Ross, B. Vogeli, M.E. Walsh, H.I. Smith, Magnetization reversal in lithographically patterned sub-200-nm Co particle arrays, J. Appl. Phys. 91 (2002) 7989.
[18] M.T. Rahman, X. Liu, A. Morisako, TbFeCo perpendicular magnetic recording media deposited on nanohole arrays of porous alumina layer, J. Appl. Phys. 99 (2006) 08G904.
[19] H. Chik, J.M. Xu, Nanometric superlattices: non-lithographic fabrication, materials, and prospects, Mater. Sci. Eng. R 43 (2004) 103–138.
[20] L. Piraux, V.A. Antohe, F. Abreu Araujo, S.K. Srivastava, M. Hehn, D. Lacour, S. Mangin, T. Hauet, Periodic arrays of magnetic nanostructures by depositing Co/Pt multilayers on the barrier layer of ordered anodic alumina templates, Appl. Phys. Lett. 101 (2012) 013110.
[21] M. Albrecht, G. Hu, I.L. Guhr, T.C. Ulbrich, J. Boneberg, P. Leiderer, G. Schatz, Magnetic multilayers on nanospheres, Nat. Mater. 4 (2005) 203.
[22] S. Oikawa, T. Onitsuka, A. Takeo, M. Takagishi, Flat surface percolated perpendicular media with metal, IEEE Trans. Magn. 48 (2012) 3192.
[23] R. Law, R. Sbiaa, T. Liew, T.C. Chong, Effect of Ta seed layer and annealing on magnetoresistance in CoFe/Pd based pseudo-spin-valves with perpendicular anisotropy, Appl. Phys. Lett. 91 (2007) 242504.
[24] T. Tahmasebi, S.N. Piramanayagam, R. Sbiaa, R. Law, T.C. Chong, Effect of different seed layers on magnetic and transport properties of perpendicular anisotropic spin valves, IEEE Trans. Magn. 46 (2010) 1933.
[25] A. Maximenko, J. Fedotova, M. Marszałek, A. Zarzycki, Y. Zabila, Magnetic characteristics of CoPd and FePd antidots arrays on nanoperforated Al_2O_3 templates, J. Magn. Magn. Mater. 400 (2016) 200–205.
[26] A. V. Naumkin, A. Kraut-Vass, S. W. Gaarenstroom, and C. J. Powell, NIST Standard Reference Database 20 (NIST X-ray Photoelectron Spectroscopy Database), Version 4.1, https://srdata.nist.gov/xps/Default.aspx.
[27] P.J. Godowski, T. Ohgi, D. Fujita, Surface segregation of CoPt polycrystalline alloy, Acta Phys. Pol. A 104 (2003) 35.
[28] L. Arroyo-Ramírez, R. Montano-Serrano, R.G. Raptis, C.R. Cabrera, Nanostructural formation of Pd-Co bimetallic complex on HOPG Surfaces: XPS and AFM studies, Res. Lett. Nanotechnol. 2009 (2009), 971423.
[29] C. Schulze, M. Faustini, J. Lee, H. Schletter, M.U. Lutz, P. Krone, M. Gass, K. Sader, A.L. Bleloch, M. Hietschold, M. Fuger, D. Suess, J. Fidler, U. Wolff, V. Neu, D. Grosso, D. Makarov, M. Albrecht, Magnetic films on nanoperforated templates: A route towards percolated, Nanotechnology 21 (2010) 495701.
[30] J. Carrey, E.A. Berkowitz, W.F. Egelhoff Jr., D.J. Smith, Influence of interface alloying on the magnetic properties of Co/Pd multilayers, Appl. Phys. Lett. 83 (25) (2003) 5259.
[31] M. Gottwald, K. Lee, J.J. Kan, B. Ocker, J. Wrona, S. Tibus, J. Langer, S.H. Kang, E.E. Fullerton, Ultra-thin Co/Pd multilayers with enhanced high-temperature annealing stability, Appl. Phys. Lett. 102 (2013) 052405.
[32] ICDD Card 00-050-1437.
[33] J.V. Kasiuk, A.A. Maksimenko, J.A. Fedotova, M. Marszalek, S.K. Lazaruk, O.V. Kupreeva, Effect of the morphology on the mechanisms of the magnetization

reversal of multilayered thin Co/Pd films, Phys. Sol. Stat. 58 (11) (2016) 2312–2319.
[34] ICDD Card 00-001-1190.
[35] ICDD Card 00-001-1194.
[36] ICDD Card 00-029-0499.
[37] X. Sun, Z.Y. Jia, Y.H. Huang, J.W. Harrell, D.E. Nikles, K. Sun, L.M. Wang, Synthesis and magnetic properties of CoPt nanoparticles, J. Appl. Phys. 95 (2004) 6747.
[38] E.C. Stoner, E.P. Wohlfarth, A mechanism of magnetic hysteresis in heterogeneous alloys, Phil. Trans. Roy. Soc. A 240 (1948) 599–642.
[39] M.T. Rahman, R.K. Dumas, N. Eibagi, N.N. Shams, Y.–Ch. Wu, K. Liu, Ch.-H. Lai, Controlling magnetization reversal in Co/Pt nanostructures with perpendicular anisotropy, Appl. Phys. Lett. 94 (2009) 042507.
[40] E. Kondorski, J. Phys. (USSR) 2 (1940) 161.
[41] D. Spenato, V. Castel, S.P. Pogossian, D.T. Dekadjevi, J.B. Youssef, Asymmetric magnetization reserval behavior in exchange-biased NiFe/MnPt bilayers in two different anisotropy regimes: close and far from critical thickness, Appl. Phys. Lett. 91 (2007) 062515.
[42] A. Hoffmann, M. Grimsditch, J.E. Pearson, J. Nogues, W.A.A. Macedo, I.K. Schuller, Tailoring the exchange bias shape anisotropy in ferromagnetic/antiferromagnetic exchange-coupled systems, Phys. Rev. B 67 (2003) 220406(R).
[43] S.H. Chung, A. Hoffmann, M. Grimsditch, Interplay between exchange bias and uniaxial anisotropy in a ferromagnetic/antiferromagnetic exchange-coupled system, Phys. Rev. B 71 (2005) 214430.